SF2A 2025
A. Siebert, K. Baillié, M. Béthermin, F. Cantalloube, E. Josselin, N. Lagarde, J. Malzac, J. Richard, L. Selliez, O. Venot (eds)

LOCATING THE EARTH'S MAGNETOPAUSE THROUGH X-RAY IMAGING

P. Boskou[1], D. Koutroumpa[1], R. Modolo[1] and Q. Xu[1]

Abstract.
Despite the development of several empirical magnetopause models based on statistical analyses of in-situ crossings, capturing the global dynamics of the magnetopause remains a significant challenge. The goal of the current study is to develop a methodology that probes the global dynamics of the magnetopause by utilizing the remote sensing capabilities of the Soft X-ray Imager (SXI) onboard the SMILE (Solar wind Magnetosphere Ionosphere Link Explorer) mission. In this context, the team has developed the Dynamic LATMOS Test Particle (DLaTeP) model, which estimates the flux in the Earth's magnetosheath and produces synthetic images representative of SXI observations. We propose a methodology and a pipeline based on synthetic images to fit empirical magnetopause models, in order to retrieve the instantaneous location and topology of the magnetopause from single SXI images. From the fitted parameters, we reconstruct the magnetopause surface, providing information about its location and shape.

Keywords: Magnetopause, Charge-exchange, Tangent Fitting, DLaTeP

1 Introduction

Understanding the shape and location of the magnetopause is crucial to explaining the dynamics and processes of geophysical plasmas, and particularly the response of the magnetosphere to the solar wind forcing. This has been studied extensively through in-situ measurement techniques, by performing statistical analyses of multiple satellite crossings (Nguyen et al. 2022). However, deriving global dynamics of a boundary from localized measurements alone is a challenging task, raising the need for remote-sensing capabilities. This is the premise of the SMILE (Solar wind Magnetosphere Ionosphere Link Explorer) mission, which aims to image the magnetopause by utilizing the Solar Wind Charge-exchange X-ray (SWCX) emission process between the heavy ions of the solar wind and the hydrogen geocoronna. (Wang et al. 2025). The X-rays that are produced from this process are captured by the Soft X-ray Imager (SXI) on-board (Sembay et al. 2024).

In preparation for this mission the LATMOS team has developed the Dynamic LATMOS Test Particle (DLaTeP) model, a test particle model with input electric (E) and magnetic (B) fields from MHD (OpenGGCM/PPMLR) simulations, that is capable of estimating the X-ray flux in the Earth's magnetosheath. In the DLaTeP model, we launch numerical test-particles, representing ions, solving their motion equation as they propagate in the MHD-computed E and B fields, and calculate the probability of them charge exchanging with the hydrogen geocorona. The E/B fields themselves are being updated every 1 minute and are linearly interpolated in time, while new particles are being launch every 0.05 second (Xu et al. (in review)).

We can integrate the X-ray volume emissivity Q $[eVcm^{-3}s^{-1}]$ calculated in the simulation, along a specific Line Of Sight (LOS) to obtain the intensity I of each looking direction in $eVcm^{-2}s^{-1}sr^{-1}$. We also assume isotropic emission and divide by 4π to get the emissivity in a particular direction.

$$I = \frac{1}{4\pi} \int_{LOS} Q \, ds \tag{1.1}$$

Calculating this quantity for each pixel's LOS of the imager, we can construct a synthetic image of the expected SXI data. This does not take into account the contribution from background sources nor the response of the instrument (Snowden et al. 1997; Sembay et al. 2024).

[1] LATMOS, 78280 Guyancourt, France

Having constructed the synthetic images, we can develop methods to analyse them. When attempting to extract three-dimensional information from a two-dimensional image, however, one must make a set of assumptions to account for this loss of information. In this end, three notable techniques have been proposed to reconstruct the magnetopause using soft X-ray imaging (Jorgensen et al. 2019; Collier & Connor 2018; Sun et al. 2020). In this study we propose a variation of the Tangent Fitting Approach (TFA) introduced by Sun et al. (2020). The relevant code and documentation are available here.

2 Method

When trying to extract 3D information from a 2D image, we need to make some assumptions to account for the loss of information from the integration over the third axis. In the TFA we assume that the tangent direction of the magnetopause coincides with the maximum intensity arc of the integrated image. This hypothesis is based on the idea that under homogeneous emission, the longest path of integration will result in the brightest features. However, this does not hold true for every satellite position, as tackled by Read (2024). In this study we are going to investigate solely observers at infinity along the Z and Y axis, where this hypothesis has been verified (Sun et al. 2020; Samsonov et al. 2022).

We can then attempt to reconstruct the 3D information by assuming a particular shape for the magnetopause - an empirical model. A first approach could be, to trace the maximum intensity arc and then try to fit the model parameters to the arc, for that particular Point Of View (POV). However, extracting a clean curve that follows the intended shape is not a simple extraction of the maximum intensity per row. We should also remember that the images that we are analyzing do not include any instrumental noise, background contributions or binning of the resolution. The SXI team has developed the relevant tools, not only to simulate the expected noise and background, but also to subtract it from the final images and aid in their processing. In any case, the expected images will display complex structures either due to kinetic effects or the instrument's response and noise, leading to the need for a robust detection method under these conditions.

The method that will be described in this section was inspired by a feature extraction technique used in image processing - the Hough Transform (Hough 1962). The Hough Transform is typically used in image analysis to find imperfect instances of shapes by a voting procedure, from which object candidates are obtained as local maxima in the parameter space. To create this shape instance, we need an analytical function that can be discretized in order to transform from image to parameter space and vise-versa. Here, we develop a Hough-like voting method, by introducing the projection of an empirical model as the analytical function. The voting is performed using directly the mean intensity of the image along the projected lines, since we are searching for the most bright instances.

We will demonstrate the methodology using the simplest empirical model, the Shue model (Shue et al. 1997). We generate a set of Shue surfaces for a range of the model's parameters, r_0 and α. Due to its rotationally symmetrical nature, the projection of the tangent direction for an observer at infinity of the Z or Y axis, is the Shue model expression itself :

$$r(\theta, \phi) = r_0 \left(\frac{2}{1 + \cos\theta} \right)^{\alpha}$$

We convert this set of curves into GSE coordinates and rasterize them according to the grid of the integrated images of the emissivity cubes. For each curve, we can calculate the mean intensity of the integrated image along its path, and use this as a metric of the curve's brightness. Each curve corresponds to a set of r_0 and α, meaning that we can plot this metric of each curve in the parameter space as shown in Fig 1 (Left). The coordinates of the maximum value in parameter space, correspond to the most prominent Shue projection. Transforming back to the image space we plot this projection with red, as in Fig 1 (Right).

3 DLaTeP Results

To demonstrate this method we will use as input to the DLaTeP model the electro-magnetic field data derived from PPMLR MHD model for a real-time IMF southward turning event recorded by WIND on 17th, March, 2015 from 07:25 UT to 07:55 UT. There is a strong IMF southward turning (from $\sim nT$ to $\sim 19nT$) during this period while the density, bulk velocity, and thermal velocity are relatively stable. We can run this pipeline for each timestep, using the images constructed from the integration of the output emissivity cubes. Figure 1 shows the Point Of View (POV) of an observer at infinity along the Z-axis, while Figure 2 shows the integration over the Y-axis. In both cases the red line indicates the result of the Shue model Hough transform. The black

points indicate the position of the magnetopause extracted directly from the simulation cube by taking the limit of the open-closed magnetic field lines, as it was also performed in Xu et al. (2025, in review). Limited points were available, especially in the Y-axis cut where the geometry is more complex, where we plot only the sub-solar point. Information about the true flaring parameter can also not be extracted reliably, due to this limited number of points. We therefore focus on quantifying the sub-solar distance performance, and treat the flaring qualitatively.

In the Z-axis integration we find good agreement between the Hough-fitted model and the cube-extracted model. This is not surprising considering that the Shue model was constructed solely by crossings of a satellite in equatorial orbit, and therefore describes this plane accurately. This highlights the success of the method when utilizing a representative empirical model.

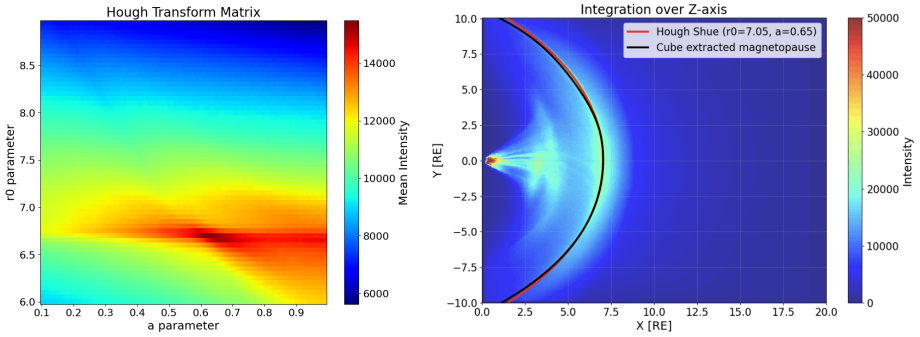

Fig. 1. Left: Visualization of the Hough transform parameter space of the Shue model for the instant T = 0 min. The colorscale represents the mean SWCX X-ray intensity along the Shue model projections in $[eVcm^{-1}s^{-1}sr^{-1}]$. **Right:** Integration of the SWCX volume emissivity over the Z-axis of the D-LaTeP simulation box for the instant T = 0 min. The colorscale represents the X-ray intensity in $[eVcm^{-2}s^{-1}sr^{-1}]$. The red curve represents the Hough-derived best Shue projection of the magnetopause. The black curve represents the magnetopause extracted from the MHD simulation.

However, when moving to the Y-axis POV, the Shue model fails to capture the complexity of the magnetopause surface, as it can not describe the indentation of the cusps or any asymmetry. This leads to the flaring parameter capturing sometimes the inner cusp boundary (Fig 2 Left) and other times the outer magnetopause (Fig 2 Right), depending on the solar wind conditions. Other empirical models available in the community, although including a description of the cusps, do not predict such a prominent indentation. Such models, with a more sophisticated parametrization, shall be tested. In order to extract the maximum information from such viewing angles, new models could also be constructed and parametrized based on the simulation.

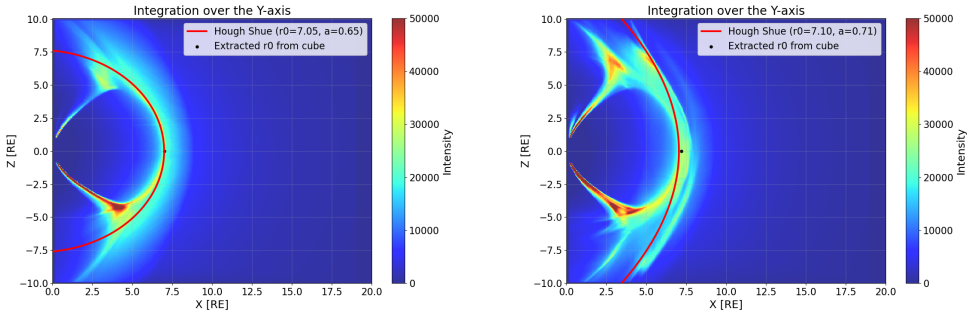

Fig. 2. Same as in Fig. 1-Right, except the integration is over the Y-axis, for two different instants of the simulation run. The red curve represents the Hough-derived best Shue projection of the magnetopause, while the black dot represents the subsolar magnetopause point extracted from the MHD cube.

Taking these limitations into account, we can still extract useful information about the magnetopause subsolar distance - one of the main objectives of the mission. In Fig. 3 we present the time evolution of the estimated r_0 (left panel), as well as the relative error to the cube-extracted sub-solar point (right panel). The

mean error for the Z integration is $0.077 \pm 0.05RE$ while for the Y integration $0.11 \pm 0.08RE$, going in both cases well below the $0.5RE$ requirement of the mission.

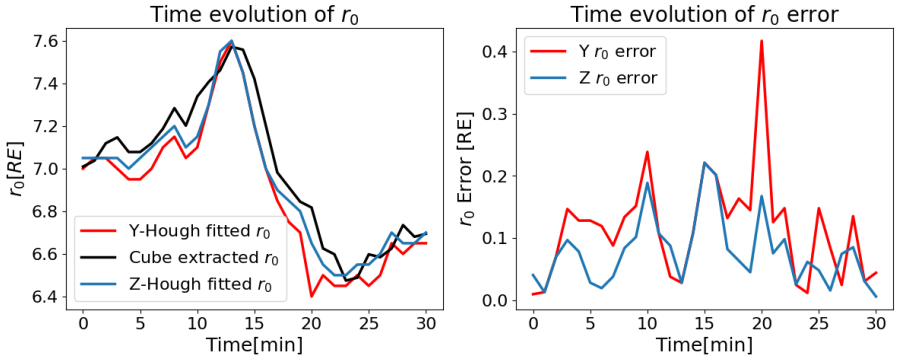

Fig. 3. Left: Time evolution of the estimated r_0 for the duration of the simulation run. **Right:** Time evolution of relative error to the cube-extracted sub-solar point.

4 Discussion

We have successfully developed a robust method to support the implementation of the tangent fitting approach in structured images. This can be implemented for images in-orbit by introducing a way to project the models to the FOV for each satellite position (implementation & documentation). However, the validity of the tangent hypothesis is not guaranteed for every POV, making the method limited to specific observational geometries. The observer at infinity chosen above ensures a simplified version of the problem, allowing for the investigation of the limitations of the method itself.

It is obvious that the main limitation is the empirical model that is chosen, as seen by the difference in the performance of the two viewing directions. The Y-axis observer is of particular interest, since a similar POV will be facilitated by the Lunar Environment heliospheric X-ray Imager (LEXI), a wide field-of-view soft X-ray telescope that was deployed on the lunar surface in 2025 (Walsh et al. 2024). To support such missions, different models should be developed and characterized, especially focusing on the cusp region where precipitating particles lead to prominent X-ray emission regions, not described by current empirical magnetopause models.

Acknowledgements

This work was supported by CNES. The authors wish to thank the SXI team at Leicester for useful discussions. We are also grateful to the Centre de Données de la Physique des Plasmas (CDPP) and the 3DView team for developping the SWCX map integration tool.

References

Collier, M. R. & Connor, H. K. 2018, Journal of Geophysical Research: Space Physics, 123

Hough, P. V. 1962, METHOD AND MEANS FOR RECOGNIZING COMPLEX PATTERNS, uS Patent 3,069,654

Jorgensen, A. M., Sun, T., Wang, C., et al. 2019, Journal of Geophysical Research: Space Physics, 124, 4365

Nguyen, G., Aunai, N., Michotte De Welle, B., et al. 2022, Journal of Geophysical Research: Space Physics, 127

Read, A. 2024, Earth and Planetary Physics, 8, 155

Samsonov, A., Sembay, S., Read, A., et al. 2022, Journal of Geophysical Research: Space Physics, 127

Sembay, S., L. Alme, A., Agnolon, D., et al. 2024, Earth and Planetary Physics, 8, 5

Shue, J.-H., Chao, J. K., Fu, H. C., et al. 1997, Journal of Geophysical Research: Space Physics, 102, 9497

Snowden, S. L., Egger, R., Freyberg, M. J., et al. 1997, The Astrophysical Journal, 485, 125

Sun, T., Wang, C., Connor, H. K., Jorgensen, A. M., & Sembay, S. 2020, Journal of Geophysical Research: Space Physics, 125

Walsh, B. M., Kuntz, K. D., Busk, S., et al. 2024, 220, 37

Wang, C., Branduardi-Raymont, G., Escoubet, C. P., & Forsyth, C. 2025, Space Science Reviews, 221